# Supporting Information

## Chirality Control in *in-situ* Preparation of Gold Nanoparticle Superstructures Directed by a Coordinatable Organogelator

Liangliang Zhu,[†] Xin Li,[‡] Shaojue Wu,[†] Kim Truc Nguyen,[†] Hong Yan,[†] Hans Ågren,[‡] and Yanli Zhao[*,†,#]

[†]Division of Chemistry and Biological Chemistry, School of Physical and Mathematical Sciences, Nanyang Technological University, 21 Nanyang Link, Singapore 637371

[‡]Department of Theoretical Chemistry and Biology, School of Biotechnology, KTH Royal Institute of Technology, SE-10691 Stockholm, Sweden

[#]School of Materials Science and Engineering, Nanyang Technological University, 50 Nanyang Avenue, Singapore 639798

To whom correspondence should be addressed

Professor **Yanli Zhao**
Division of Chemistry and Biological Chemistry
School of Physical and Mathematical Sciences
Nanyang Technological University
21 Nanyang Link
Singapore 637371
E-mail: zhaoyanli@ntu.edu.sg
Phone: 65-63168792
Homepage: http://www.ntu.edu.sg/home/zhaoyanli/

# *List of Content*

**Measurement of critical aggregation concentration and critical micelle concentration of SAC:**

Critical aggregation concentration (CAC) and critical micelle concentration (CMC) can be determined by measuring micelle-influenced properties.[S1] For simple operations and precise readings, we employed a method of the concentration dependence on absorbance to measure the CAC and CMC of SAC. Figure S1 exhibits the changes of the maximum absorption around 330 nm with the concentration variation of SAC at room temperature. With the difference of the molar absorption coefficient among the monomeric and different self-assembly states, the absorbance curves show different slopes below and above the CAC/CMC. The concentrations corresponding to the intersection-points indicate the CAC (10.5 μM) and CMC (0.42 mM), respectively.

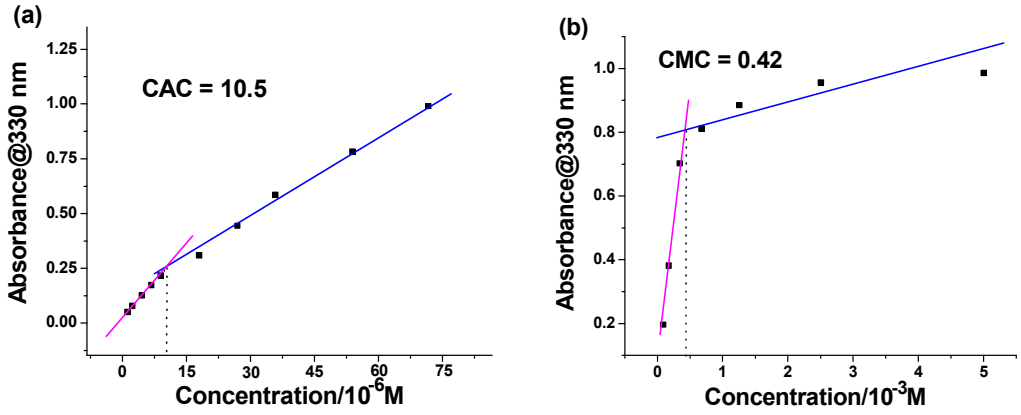


**Figure S1.** Dependence of the maximum absorbance on the concentration of SAC (298K). The data in (a) were collected in a cuvette with a path length of 10 mm at 298 K, while those in (b) were acquired in a cuvette with a path length of 1 mm at 298 K.

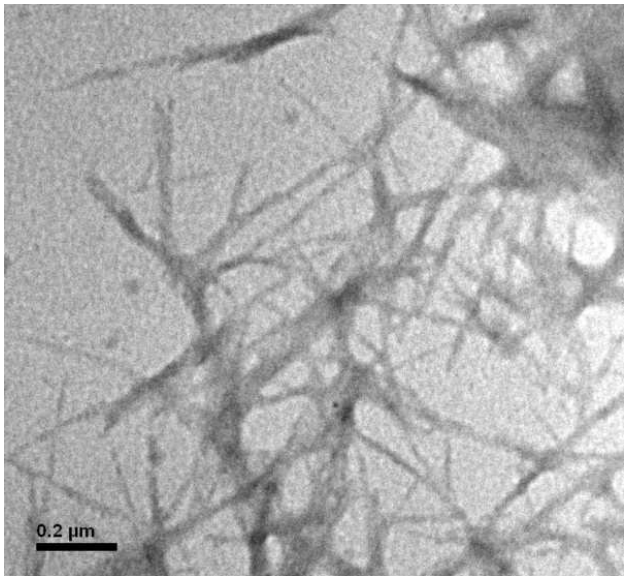


**Figure S2.** TEM image of SAC prepared from *n*-butanol solution with a concentration above CMC.

**Observation for the critical gelation concentration:**

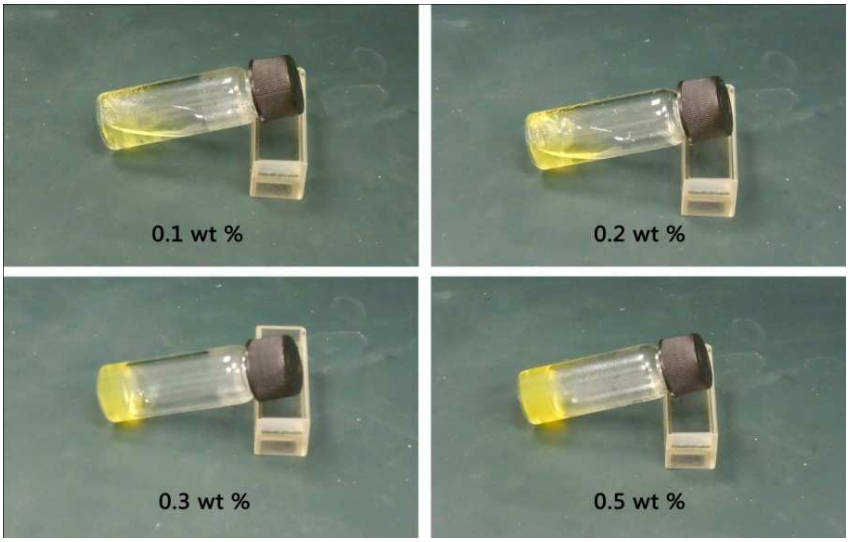


**Figure S3.** Observation for the critical gelation concentration (CGC = ~ 0.3 wt%) at room temperature: the photographs of SAC in *n*-butanol with different concentrations.

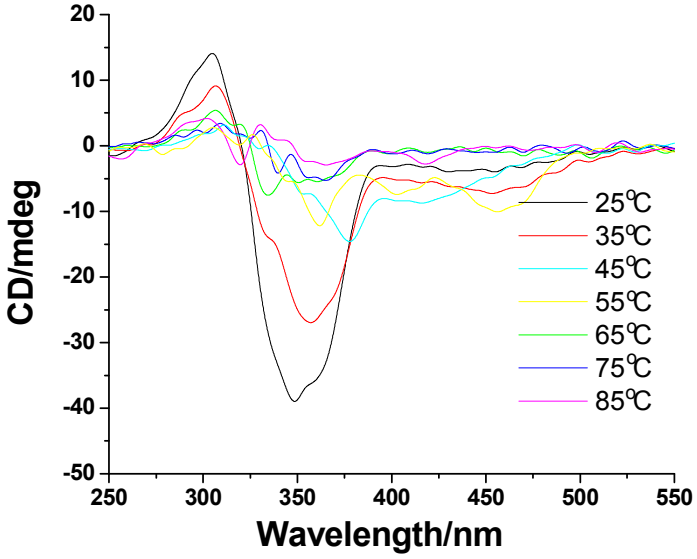


**Figure S4.** CD spectra from *n*-butanol solution of SAC at different temperatures. These spectra were determined with the concentration of 0.03 mM calculated from the azobenzene unit in a cuvette with a path length of 10 mm at 298 K.

**Coordination studies between SAC and Au(III):**

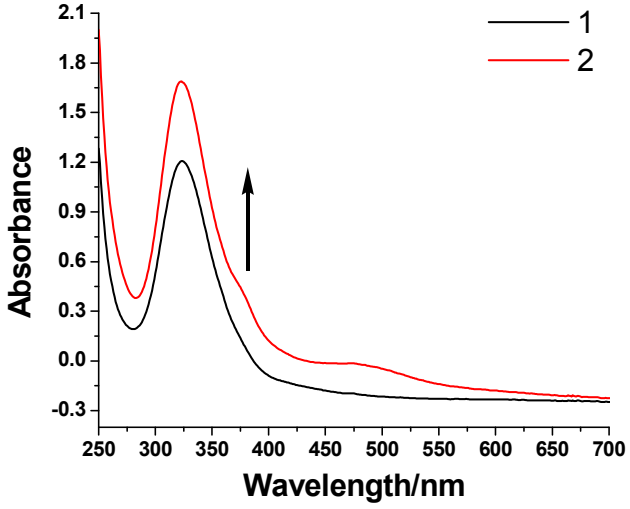


**Figure S5.** Absorption spectra for a dilute *n*-butanol solution of SAC-Sol (curve 1) before and after (curve addition of 5 eq. of $HAuCl_4$. The spectra were determined with the concentration of 0.3 mM calculated the azobenzene unit in a cuvette with a path length of 1 mm at 298 K.

**Table S1.** The absorption shift studies for different species under different conditions.

| Entry | Substrate | Addition | Solvent | Absorption Shift |
|---|---|---|---|---|
| **1** | SAC | $HAuCl_4$ | *n*-butanol | YES |
| **2** | SAC | TFA | *n*-butanol | No |
| **3** | SA | $HAuCl_4$ | *n*-butanol | YES |
| **4** | AC | $HAuCl_4$ | *n*-butanol | YES |
| **5** | SAC | $HAuCl_4$ | toluene | YES |
| **6** | lipoic acid | $HAuCl_4$ | *n*-butanol | No |
| **7** | lipoic acid | $HAuCl_4$ | toluene | No |
| **8** | cholesterol | $HAuCl_4$ | *n*-butanol | No |
| **9** | cholesterol | $HAuCl_4$ | toluene | No |

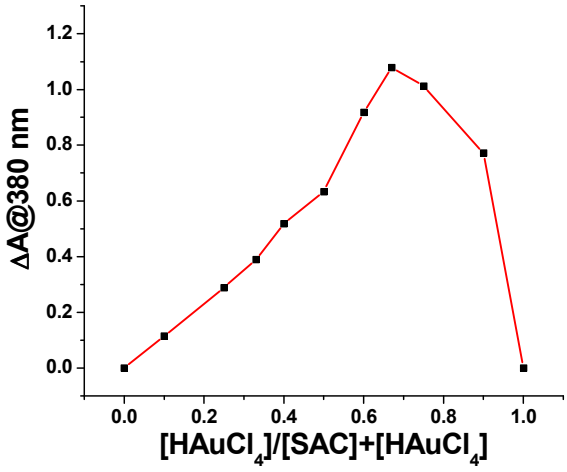


**Figure S6.** Job plot showing 1:2 stoichiometry of the coordination interaction between SAC and $HAuCl_4$ in *n*-butanol. The total concentration of the host and guest was kept at 0.4 mM.

**Complexation constant *K* between SAC and $HAuCl_4$:**[S2]

The complexation constant K between SAC and $HAuCl_4$ in n-butanol was determined by following the UV-Vis absorption changes at 470 nm as shown in Figure S7. The concentration of SAC maintains unchanged at 0.2 mM. Upon addition of $HAuCl_4$, the absorption at 470 nm changes remarkably. With a 1:2 stoichiometry, the complexation between SAC and $HAuCl_4$ is expressed by the following equation:

$$[SAC] + [Au(III)] \underset{}{\overset{k_1}{\rightleftharpoons}} [Au(III)\text{-}SAC]$$

$$[Au(III)\text{-}SAC] + [Au(III)] \overset{k_2}{\rightleftharpoons} [2Au(III)\text{-}SAC]$$

$$K = k_1 k_2$$

We employed the double reciprocal plot in the calculation of the complexation constant K according to the modified Hidebrand-Benesi equation:

$$\frac{1}{[\Delta A]} = \frac{1}{K\,[\Delta\varepsilon][SAC]\,[Au(III)]^2} + \frac{1}{[\Delta\varepsilon][SAC]}$$

Where ΔA denotes the absorbance difference before and after addition of $HAuCl_4$ and Δε denotes the difference of the molar extinction coefficient between SAC and the complex at the same wavelength. The complexation constant K is calculated from the double reciprocal plot of $1/\Delta A$ versus $1/[Au(III)]^2$, and the value calculated is $6139 \pm 255\ M^{-2}$ for the coordination complex.

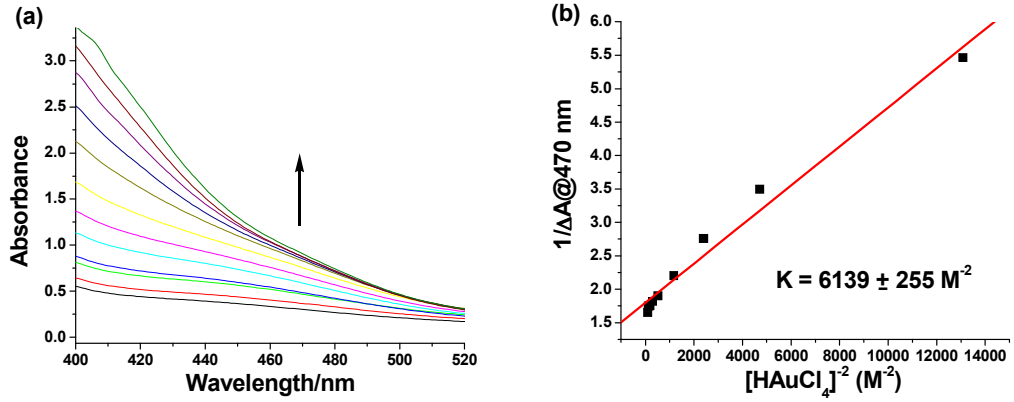


**Figure S7.** (a) UV-Vis absorption changes and (b) double reciprocal plot of SAC upon stepwise addition of $HAuCl_4$. The concentration of SAC maintains 0.2 mM.

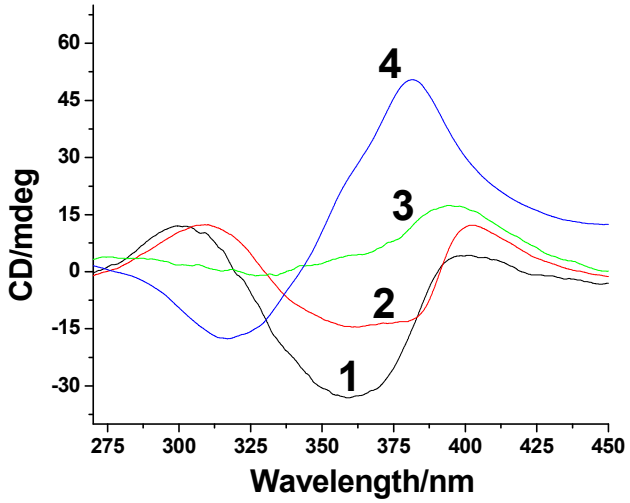


**Figure S8.** CD spectra of *n*-butanol solution of SAC-Sol after addition of (curve a) 0 eq., (curve b) 1 eq., (curve c) 2 eq. and (curve d) 5 eq. of $HAuCl_4$. The spectra were determined with the concentration of 0.3 mM calculated from the azobenzene unit in a cuvette with a path length of 1 mm at 298 K.

**Supplementary computational results:**

In molecular dynamics (MD) simulations the SAC or 2Au(III)-SAC molecules were simulated in high-polarity environment to ensure fast formation of self-assemblies in the time scale of several tens of nanoseconds. In aqueous solution, the ten SAC molecules quickly assembled together to form a helical self-assembly (Figure S9), and the order parameter[S3] of the molecules sharply increased from ~0.35 to ~0.70 during 5−10 ns and finally reaches ~0.85 in the time interval of 40−50 ns (Figure S10). Such a large value of order parameter (close to 1) indicates the highly ordered structure of the self-assembly consisting of SAC molecules. Differently, SAC molecules in methanol solution showed a much slower formation of self-assembly, as reflected by the fact that the order parameter gradually increases from ~0.10 to ~0.45 during 10−65 ns (Figure S10). The snapshots in Figure S9 show that in aqueous solution all the ten SAC molecules aggregated together, and that only five SAC molecules were involved in the self-assembly in

methanol solution. Nonetheless, the computed ECD spectra by the semi-empirical ZIndo/S method suggest that the SAC self-assembly formed in methanol exhibits similar optical rotation properties to that in aqueous solution (Figure S9). The ECD signals of SAC assembly suggest formation of an *M*-helix. Furthermore, the accuracy of the semi-empirical ZIndo/S method was assessed by comparison with the more accurate TDDFT calculations. Two SAC dimers were extracted from one snapshot of the SAC self-assembly in methanol solution, and their computed ECD spectra are shown in Figure S11. It is found that the ZIndo/S method produces almost the same line shape of the ECD spectra as TDDFT but underestimates the excitation energies at ECD peaks and troughs; thus the ECD spectra computed by the ZIndo/S method has to be corrected by a ~40 nm shift towards shorter wavelength. Applying such a correction to the ECD spectra in Figure S11 leads to a better agreement between the experimentally measured spectra and calculated spectra.

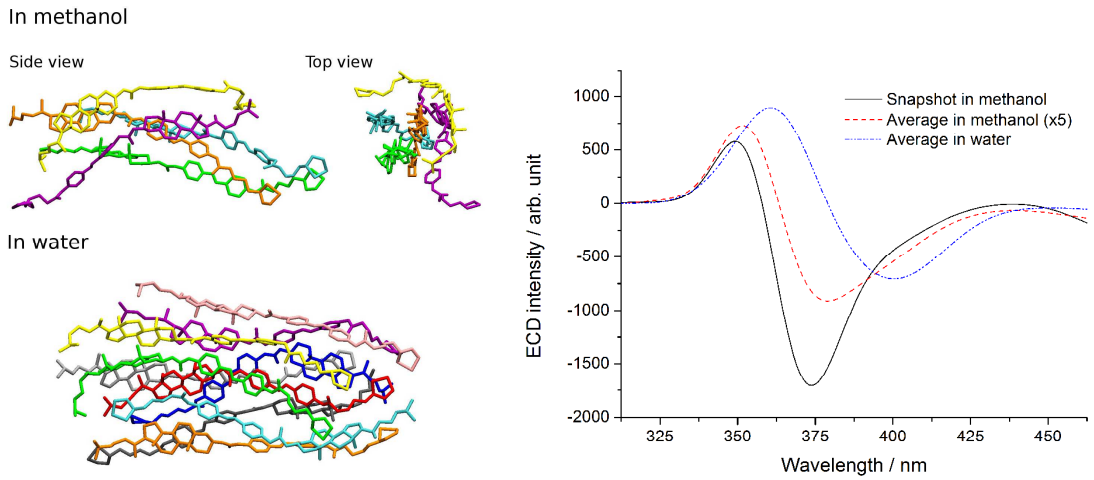


**Figure S9.** (left) Snapshots of SAC self-assemblies in methanol and aqueous solution. (right) Computed ECD spectra (ZIndo/S method) averaged over the last 10 ns of simulation trajectories.

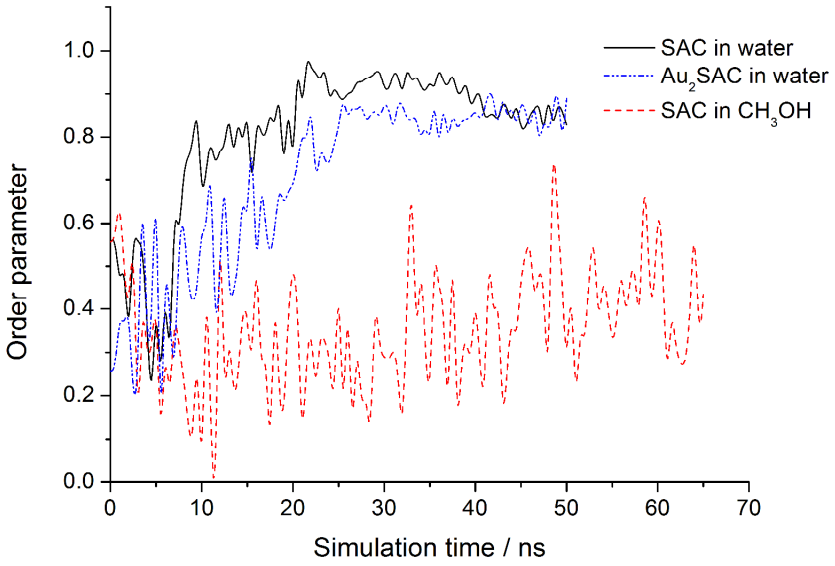


**Figure S10.** Time evolution of order parameter of SAC in water, 2Au(III)-SAC in water and SAC in methanol.

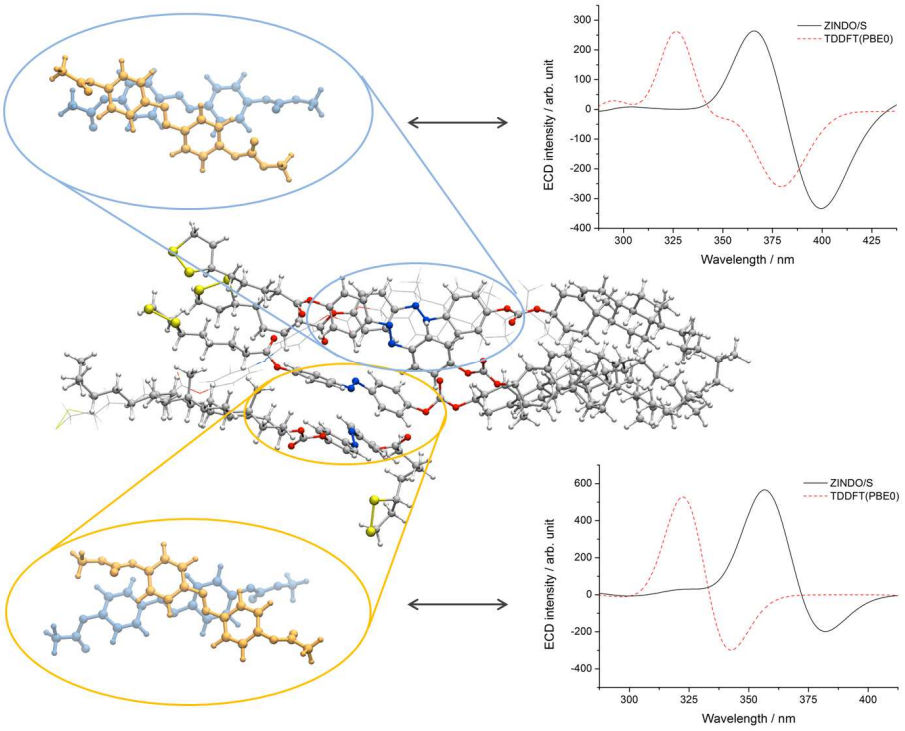


**Figure S11.** Snapshot of SAC assembly in methanol with two well-stacked SAC dimers and their computed ECD spectra.

Similar to SAC, simulations of ten 2Au(III)-SAC molecules in aqueous solution also demonstrate fast formation of self-assembly with an order parameter of ~0.85 in the time interval of 40−50 ns (Figure S10). Since the ZIndo/S method is not applicable to systems containing gold atoms, we here apply TDDFT calculations to compute the ECD spectra of the 2Au(III)-SAC self-assembly. As shown in Figure S12, two well-stacked 2Au(III)-SAC dimers were extracted from the assembly, and their computed ECD spectra were averaged over the last 10 ns trajectory. These two dimers are representatives of the 2Au(III)-SAC self-assembly and the computational costs are affordable with currently available computational resources. TDDFT calculations show that these two dimers exhibit consistent optical rotation in the region of 250−400 nm and suggest the formation of a *P*-helix (Figure S12). A comparison between the *M*- and *P*-helices is illustrated by the SAC and 2Au(III)-SAC dimers shown in Figure 4. In SAC dimer the azo (−N=N−) unit stacks over the phenyl ring through weak interaction, and the macro handedness and helicity are most likely guided by the chiral cholesterol units. However, in 2Au(III)-SAC dimer the stacking pattern and helicity are altered by the presence of the gold atoms. To further address the driving force of such a phenomenon, we analyzed the intermolecular Coulomb and van der Waals (VDW) interaction energies within the SAC and $Au_2$SAC self-assemblies (Figure S13). For both SAC and 2Au(III)-SAC, the VDW interaction energy is dominantly larger than the Coulomb interaction energy; in other words, the hydrophobic−hydrophobic attraction is the main driving force of the formation of the self-assemblies. Furthermore, it is noteworthy that from SAC to 2Au(III)-SAC the absolute values of VDW and Coulomb interaction energies increased 11% and 245%, respectively (Table S2). This result indicates that the introduction of gold and chloride atoms into SAC molecules results in significant enhancement of Coulomb attraction. As shown in Figure 3, the short distance (3.33 Å) between the gold atoms in the upper 2Au(III)-SAC unit and the chlorine atom in the lower 2Au(III)-SAC unit reflect that the electrostatic

interaction takes effect. The vertical distance between the two stacking units is around 3.6 Å in both SAC and 2Au(III)-SAC dimers, being of typical π-π stacking character.

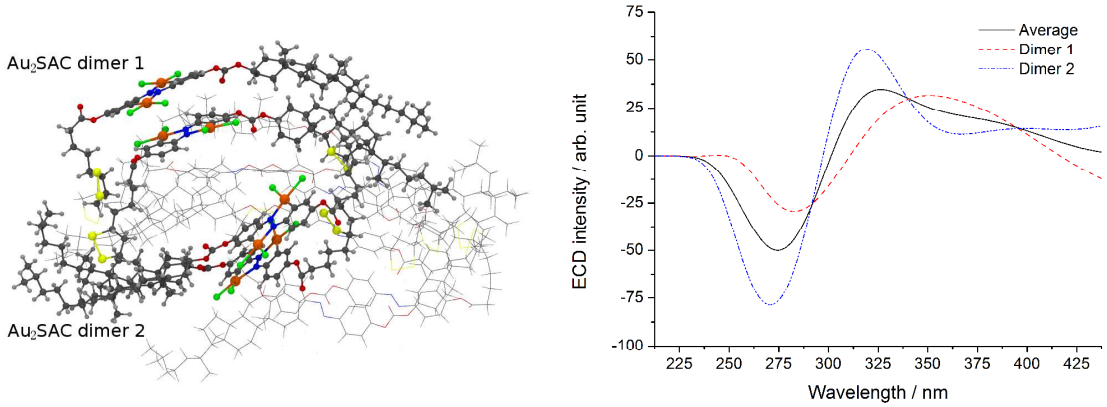


**Figure S12.** (left) Snapshot of 2Au(III)-SAC assembly in aqueous solution with the two well-stacked 2Au(III)-SAC dimers highlighted. (right) Computed ECD spectra (TDDFT method) of the two dimers and their average over the last 10 ns of simulation trajectories.

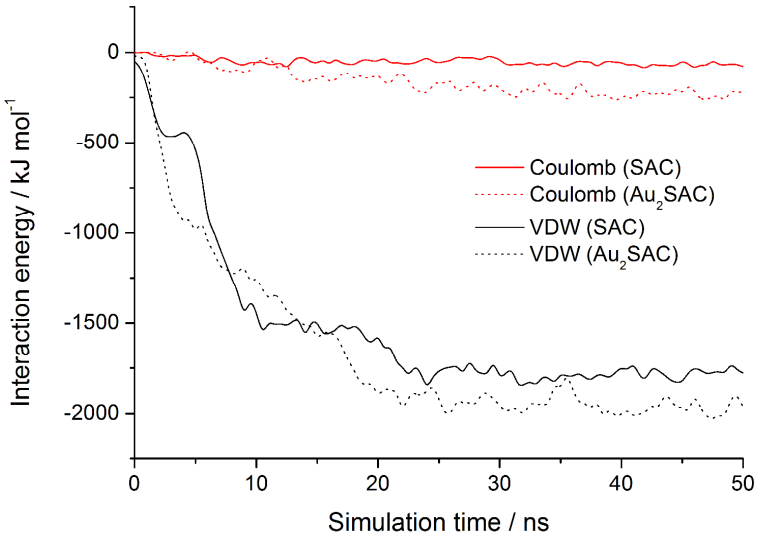


**Figure S13.** Time evolution of intermolecular Coulomb and VDW interaction energies within SAC and 2Au(III)-SAC self-assemblies in water.

**Table S2.** Intermolecular interaction energies (in kJ/mol) within SAC and 2Au(III)-SAC self-assemblies in water, averaged over 40−50 ns.

| | SAC | 2Au(III)-SAC | ΔE |
|---|---|---|---|
| E(VDW) | -1774.6 | -1970.2 | -195.6 |
| E(Coulomb) | -67.2 | -231.8 | -164.6 |

**Supplementary characterizations for the superstructures:**

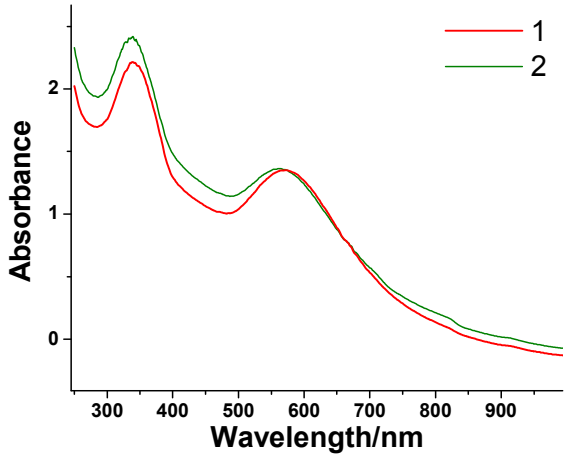


**Figure S14.** Full spectra of the absorption from *n*-butanol solutions of Au@SAC-1 (curve 1) and Au@SAC-2 (curve 2), showing both the bands from azobenzenyl chromophore and gold nanoparticles, respectively.

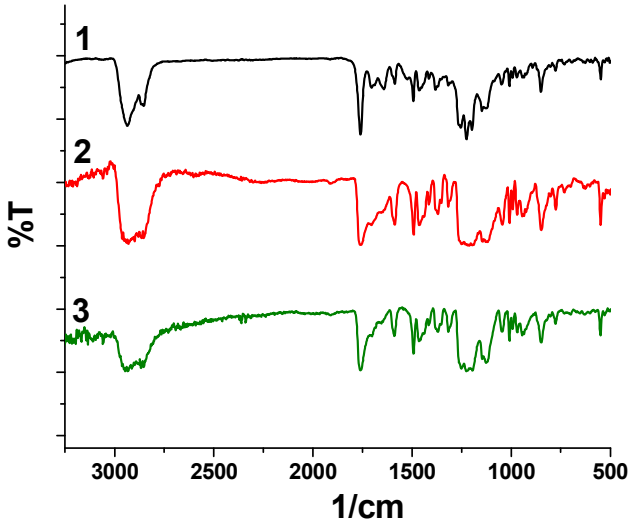


**Figure S15.** FT-IR spectra of SAC (curve 1), Au@SAC-1 (curve 2) and Au@SAC-2 (curve 3). The main peaks corresponding to the vibrations of SAC ligand in the curve 2 and 3 show slight shifts as compared to those in curve 1, indicating SAC was successfully incorporated with gold components.

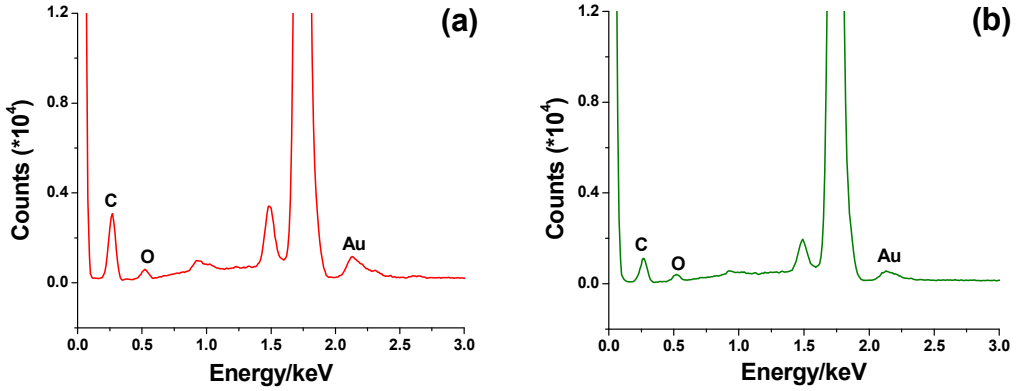


**Figure S16.** EDS spectra of (a) Au@SAC-1 and (b) Au@SAC-2. The observation of the peaks of the elements C, O, Au in these spectra suggests that both the organic and inorganic components exist in the hybrid gold nanostructures.

**Optimization for the in-situ preparation strategy:**

**Table S3.** Macrochirality of the hybrid gold nanostructures prepared under different conditions ([a] Null means that the chirality is unable to be distinguished).

| Entry | Temperature (ºC) | Addition Sequence | Macrochirality |
|---|---|---|---|
| **1** | R.T. | 1.$HAuCl_4$, 2.TBAB | M-helix |
| **2** | R.T. | 1.TBAB, 2.$HAuCl_4$ | M-helix |
| **3** | 55 | 1.$HAuCl_4$, 2.TBAB | P-helix |
| **4** | 55 | 1.TBAB, 2.$HAuCl_4$ | M-helix |
| **5** | 85 | 1.$HAuCl_4$, 2.TBAB | Null[a] |
| **6** | 85 | 1.TBAB, 2.$HAuCl_4$ | Null |

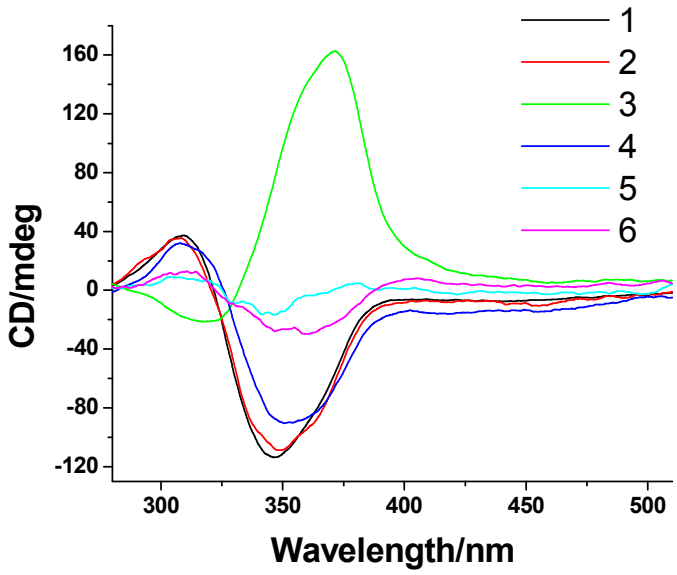


**Figure S17.** CD spectra of the hybrid gold nanostructures prepared under different conditions. The conditions for curve 1 - 6 are corresponding to 1 - 6 in Table S1, respectively.

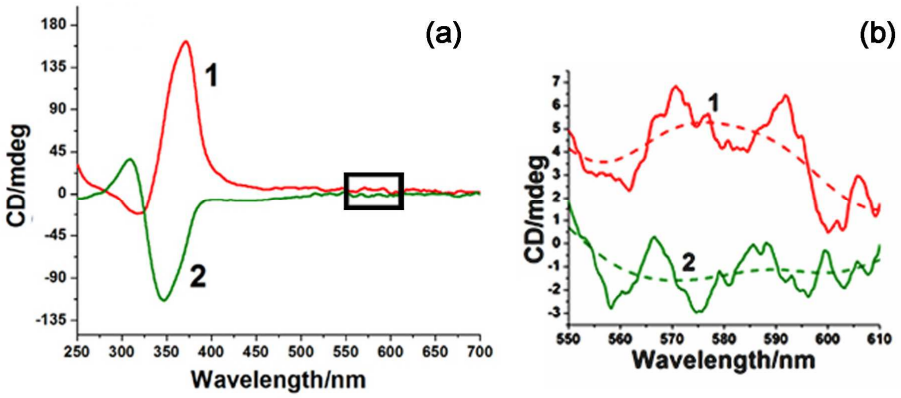


**Figure S18.** (a) CD spectra of *n*-butanol solutions of Au@SAC-1 (curve 1) and Au@SAC-2 (curve 2), (b) Plasmonic CD spectra (magnified from the rectangle in a) of *n*-butanol solutions of Au@SAC-1 (curve 1) and Au@SAC-2 (curve 2). The dash curves represent the corresponding smoothed data.

**Full citation for reference 32:**

(32) Frisch, M. J.; Trucks, G. W.; Schlegel, H. B.; Scuseria, G. E.; Robb, M. A.; Cheeseman, J. R.; Scalmani, G.; Barone, V.; Mennucci, B.; Petersson, G. A.; Nakatsuji, H.; Caricato, M.; Li, X.; Hratchian, H. P.; Izmaylov, A. F.; Bloino, J.; Zheng, G.; Sonnenberg, J. L.; Hada, M.; Ehara, M.; Toyota, K.; Fukuda, R.; Hasegawa, J.; Ishida, M.; Nakajima, T.; Honda, Y.; Kitao, O.; Nakai, H.; Vreven, T.; Montgomery Jr., J. A.; Peralta, J. E.; Ogliaro, F.; Bearpark, M.; Heyd, J. J.; Brothers, E.; Kudin, K. N.; Staroverov, V. N.; Kobayashi, R.; Normand, J.; Raghavachari, K.; Rendell, A.; Burant, J. C.; Iyengar, S. S.; Tomasi, J.; Cossi, M.; Rega, N.; Millam, J. M.; Klene, M.; Knox, J. E.; Cross, J. B.; Bakken, V.; Adamo, C.; Jaramillo, J.; Gomperts, R.; Stratmann, R. E.; Yazyev, O.; Austin, A. J.; Cammi, R.; Pomelli, C.; Ochterski, J. W.; Martin, R. L.; Morokuma, K.; Zakrzewski, V. G.; Voth, G. A.; Salvador, P.; Dannenberg, J. J.; Dapprich, S.; Daniels, A. D.; Farkas, O.; Foresman, J. B.; Ortiz, J. V.; Cioslowski, J.; Fox, D. J. *Gaussian 09*, Revision A.2, Gaussian, Inc.: Wallingford CT, **2009**.

## References:


[S1] (a) Lin, S-Y.; Lin, Y-Y.; Chen, E.-M.; Hsu, C.-T.; Kwan, C.-C. *Langmuir*, **1999**, *15*, 4370−4376; (b) Lu, H.-J.; Chen, C.; Guo, H.-T.; Zhou, X.-H.; Dong, J.-F.; Hong, X.-L.; Li, X.-F.; Zhang, G.-Y. *Acta Chim. Sinica* **2006**, *64*, 2437−2441.

[S2] (a) Benesi, H. A.; Hildebrand, J. H. *J. Am. Chem. Soc.*, **1949**, *71*, 2703−2707; (b) Hao, A-Y.; Lin, J-M.; Tong, L-H. *J. Incl. Phenom. Macrocyclic Chem*. 1999, **34**, 445−454.

[S3] Wilson, M. R. *J. Mol. Liquids* **1996**, *68*, 23–31.